

# Interannual Influences of the Surface Potential Vorticity Forcing over the Tibetan Plateau on East Asian Summer Rainfall<sup>✉</sup>

Chen SHENG<sup>1,2</sup>, Bian HE<sup>\*1,2</sup>, Guoxiong WU<sup>1,2</sup>, Yimin LIU<sup>1,2</sup>, and Shaoyu ZHANG<sup>1,2</sup>

<sup>1</sup>State Key Laboratory of Numerical Modeling for Atmospheric Sciences and Geophysical Fluid Dynamics (LASG),  
Institute of Atmospheric Physics, Chinese Academy of Sciences, Beijing 100029, China

<sup>2</sup>College of Earth and Planetary Sciences, University of Chinese Academy of Sciences, Beijing 100049, China

(Received 7 June 2021; revised 9 August 2021; accepted 13 September 2021)

## ABSTRACT

The influences of interannual surface potential vorticity forcing over the Tibetan Plateau (TP) on East Asian summer rainfall (EASR) and upper-level circulation are explored in this study. The results show that the interannual EASR and associated circulations are closely related to the surface potential vorticity negative uniform leading mode (PVNUM) over the TP. When the PVNUM is in the positive phase, more rainfall occurs in the Yangtze River valley, South Korea, Japan, and part of northern China, less rainfall occurs in southern China, and vice versa. A possible mechanism by which PVNUM affects EASR is proposed. Unstable air induced by the positive phase of PVNUM could stimulate significant upward motion and a lower-level anomalous cyclone over the TP. As a result, a dipole heating mode with anomalous cooling over the southwestern TP and anomalous heating over the southeastern TP is generated. Sensitivity experiment results regarding this dipole heating mode indicate that anomalous cooling over the southwestern TP leads to local and northeastern Asian negative height anomalies, while anomalous heating over the southeastern TP leads to local positive height anomalies. These results greatly resemble the realistic circulation pattern associated with EASR. Further analysis indicates that the anomalous water vapor transport associated with this anomalous circulation pattern is responsible for the anomalous EASR. Consequently, changes in surface potential vorticity forcing over the TP can induce changes in EASR.

**Key words:** surface potential vorticity, East Asian summer monsoon, rainfall, the Tibetan Plateau

**Citation:** Sheng, C., B. He, G. X. Wu, Y. M. Liu, and S. Y. Zhang, 2022: Interannual influences of the surface potential vorticity forcing over the Tibetan Plateau on East Asian summer rainfall. *Adv. Atmos. Sci.*, **39**(7), 1050–1061, <https://doi.org/10.1007/s00376-021-1218-4>.

## Article Highlights:

- Potential vorticity (PV), inherently combining dynamics and thermodynamics, is an ideal indicator of the full forcing of the TP.
- The leading modes of EASR and upper-level circulation are closely related to the surface PV forcing over the TP.
- We highlight that the dipole heating mode over the TP plays a critical role in the process where the TP's surface PV affects EASR.

## 1. Introduction

East Asian summer rainfall (EASR) affects East Asian countries, including China, Japan, and Korea (Ding and Chan, 2005; Kubota et al., 2016; Zhou et al., 2019). The changes and anomalies of EASR have caused frequent and severe weather disasters, including droughts, floods, and heat-waves (Huang et al., 2007, 2019). Many studies have investigated

the possible driving factors of EASR. A basic consensus is that in addition to the El Niño-Southern Oscillation (ENSO) (Wang and Zhang, 2002; Ding, 2007; Xie et al., 2016; Wen et al., 2019; Ding et al., 2020), the Indian Ocean sea surface temperature anomaly (Yang et al., 2007; Xie et al., 2009), and the Indian summer monsoon rainfall (Kripalani and Kulkarni, 1997, 2001), the Tibetan Plateau (TP; e.g., Yeh et al., 1957; Ye and Gao, 1979; Yanai et al., 1992; Liu et al., 2020) plays an important and nonnegligible role in EASR anomalies.

The TP, as the highest and broadest plateau on Earth, has increasingly attracted the attention of climatologists due to its large dynamic and thermodynamic effects on the cli-

<sup>✉</sup> This paper is a contribution to the special issue on Third Pole Atmospheric Physics, Chemistry, and Hydrology

\* Corresponding author: Bian HE

Email: [heb@lasg.iap.ac.cn](mailto:heb@lasg.iap.ac.cn)

mate of Asia. Previous studies have demonstrated that the thermal forcing of the TP can greatly impact the Asian summer monsoon system (e.g., Flohn, 1957; Yeh et al., 1957; Ye and Gao, 1979; Yanai et al., 1992; Wu et al., 1997, 2007, 2012, 2018; Xu et al., 2015). For example, Wu et al. (1997, 2007) indicated that sensible heating over the TP is the major driver of monsoon rainfall over the Asian continent. The strong surface sensible heating over the TP during boreal spring can affect the subsequent summer monsoon rainfall (Zhao and Chen, 2001; Duan et al., 2005). The onset, formation, and evolution of the Asian summer monsoon are closely related to the thermal forcing of the TP (Wu and Zhang, 1998; Hsu and Liu, 2003). Moreover, some studies have examined the mechanical effects of the TP on the Asian summer monsoon system. Hahn and Manabe (1975) documented that the South Asian summer monsoon would not reach inland Asia if the TP were removed. More complex experiments, considering increasing TP heights from zero to its contemporary height (Chen et al., 1999; Liu, 1999; Kitoh, 2004; Jiang et al., 2008), have indicated that Asian summer monsoon rainfall shifts northward from the Indian Ocean to inland Asia as TP height increases. Certain studies (Liu and Yin, 2002; Liang et al., 2005) have illustrated that the onset and evolution of the Asian summer monsoon is also sensitive to the location and height of the TP. However, little insight is given about the intrinsic combined effects of dynamic and thermodynamic forcing of the TP in the literature.

Potential vorticity (PV; Rossby, 1940; Ertel, 1942), which inherently combines atmospheric dynamics and thermodynamics, is an ideal indicator of the combined dynamic and thermodynamic conditions of the TP. Most previous studies have focused on atmospheric interior PV. Its impacts on general circulation structure (e.g., Hoskins, 1991), rainstorms, and cold air activities (e.g., Wu et al., 1995; Wu and Cai, 1997; Zhao and Ding, 2009) and its interannual relation to ozone (Danielsen, 1968; Allaart et al., 1993; Folkins and Appenzeller, 1996; Sandhya et al., 2015) and Rossby wave breaking (Folkins and Appenzeller, 1996; Ryoo et al., 2013; Bowley et al., 2019) are the main areas of interest. However, instead of atmospheric interior PV, some studies (e.g., Hoskins, 1991) highlight the importance of surface PV, especially surface PV over the TP, based on the impermeability theorem (Haynes and McIntyre, 1987, 1990). For example, the elevated TP is one of the most prominent surface PV sources in the world (Sheng et al., 2021). In particular, the surface PV over the TP (TPPV) could exert a prominent influence on the TP vortex (Sheng et al., 2021) and downstream rainfall and extreme cold events (Ma et al., 2019; Yu et al., 2019; Zhang et al., 2021). Although surface PV is known to be of great importance, the influence of surface TPPV forcing on EASR is still a knowledge gap.

This study aims to illustrate the interannual impact on EASR of the surface TPPV forcing associated with the intrinsic combined effect of the dynamics and thermodynamics of the TP. The remainder of the paper is organized as follows. Section 2 presents the data, method, and model. In section 3, the relationships of surface TPPV forcing with EASR and EASR-related circulation are presented. Section 4 analyzes the possible mechanism of how surface TPPV forcing affects EASR. Finally, conclusions and discussion are provided in section 5.

tion 3, the relationships of surface TPPV forcing with EASR and EASR-related circulation are presented. Section 4 analyzes the possible mechanism of how surface TPPV forcing affects EASR. Finally, conclusions and discussion are provided in section 5.

## 2. Data, method, and model

### 2.1. Data

Monthly mean data on the hybrid  $\sigma$ - $p$  model level obtained from MERRA2 (Rienecker et al., 2011; Lucchesi, 2012) are used to calculate surface PV and surface static stability. Variables include air temperature, zonal and meridional wind, and pressure.

Additional data used in this study include monthly outgoing longwave radiation (OLR) from the polar-orbiting series of satellites of the National Oceanic and Atmospheric Administration (Liebmann and Smith, 1996), monthly land precipitation from the Climatic Research Unit (Mitchell and Jones, 2005), and monthly specific humidity and zonal, meridional, and vertical wind on pressure level from MERRA2.

The study period is 1980–2017. The horizontal resolution of all MERRA2 data is  $0.625^\circ \times 0.5^\circ$  (longitude  $\times$  latitude). The horizontal resolutions of the OLR and precipitation data are  $2.5^\circ \times 2.5^\circ$  and  $0.5^\circ \times 0.5^\circ$ , respectively. Climate mean values calculated over June, July, and August (JJA) are used to represent the boreal summer condition.

### 2.2. Method

Surface PV is calculated as follows (Sheng et al., 2021):

$$PV = \alpha_h \xi_{ah} \cdot \nabla_h \theta = g \left[ \frac{\partial v}{\partial p} \left( \frac{\partial \theta}{\partial x} \right)_h - \frac{\partial u}{\partial p} \left( \frac{\partial \theta}{\partial y} \right)_h \right] - g \left[ f + \left( \frac{\partial v}{\partial x} \right)_h - \left( \frac{\partial u}{\partial y} \right)_h \right] \frac{\partial \theta}{\partial p}, \quad (1)$$

where  $\alpha_h$  and  $\xi_{ah}$  is the specific volume and absolute vorticity in the hybrid  $\sigma$ - $p$  coordinate system, respectively. The  $g$  is gravity, which is  $9.8 \text{ m s}^{-2}$ ,  $p$  is pressure,  $\theta$  is potential temperature,  $f$  is the Coriolis parameter,  $(u, v)$  is horizontal wind, and  $h$  indicates that the horizontal difference is carried out at the hybrid  $\sigma$ - $p$  level. The surface PV is obtained from the two bottom levels at the hybrid  $\sigma$ - $p$  level. More details about the calculation of surface PV can be found in Sheng et al. (2021).

The surface static stability is calculated as  $-\partial\theta/\partial p$ , where  $\theta$  and  $p$  are obtained from the two bottom levels at the hybrid  $\sigma$ - $p$  level.

The horizontal water vapor flux (WVF) is calculated as follows:

$$WVF = Vq = (uq, vq), \quad (2)$$

where  $q$  is specific humidity.

Statistical methods, including linear regression, linear correlation, Student's  $t$ -test, empirical orthogonal function (EOF), and multivariate EOF (MVEOF), are used in this

study. The linear trends and decadal variation (more than nine years) in the data are removed to highlight the interannual variability.

### 2.3. Model

The linear baroclinic model (LBM) (Watanabe et al., 1999; Watanabe and Kimoto, 2000) is employed to investigate the responses of the upper-level circulation to the surface PV forcing over the TP. The model used in this study has 20  $\sigma$  vertical levels. Each horizontal level is represented by spherical harmonics with a resolution of T42. More details about the model description can be found in Watanabe and Jin (2003). The LBM is a time-varying model that linearizes the basic state based on primitive equations. We take boreal summer climatology as the basic state in this study. Since dissipation terms including biharmonic horizontal diffusion, weak vertical diffusion, Newtonian

damping, and Rayleigh friction are adopted, the model response reaches its steady state at approximately 14 days. Therefore, we use the results averaged from the last 15 days in the 30-day integration for analysis.

## 3. Results

### 3.1. Leading mode of surface TPPV, EASR, and upper-level circulation

EOF analysis is applied to analyze the dominant temporal and spatial features of the surface TPPV, EASR, and circulation over East Asia during boreal summer for the 1980–2017 period. Figure 1a shows the first leading mode of the EOF (EOF1) on the summer surface TPPV. The variation in surface PV on the southern slope and in the southeastern corner of the TP has the opposite sign to that in the main TP platform. Although the signs of the surface PV in the

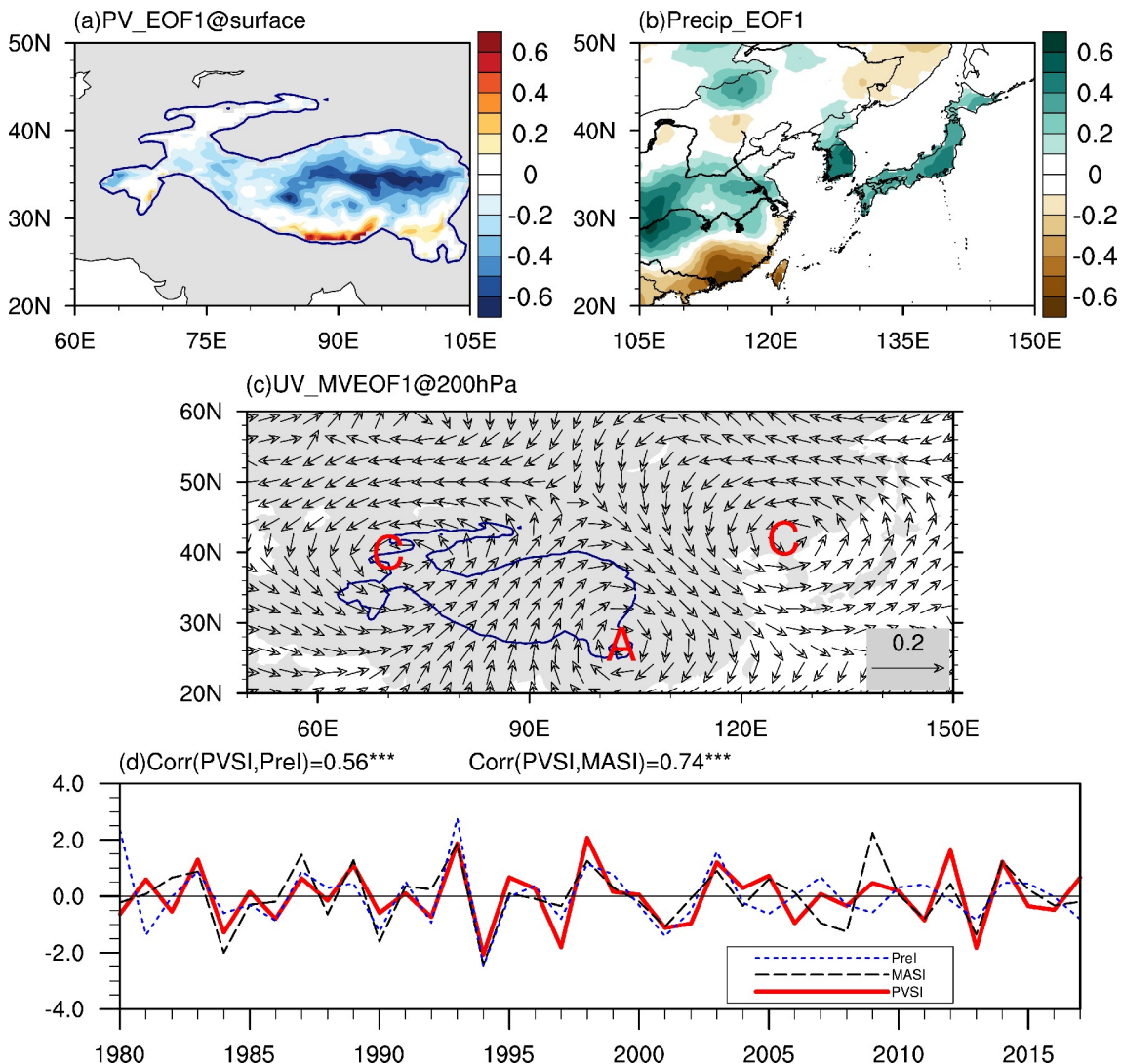


**Fig. 1.** Spatial distribution of the first leading mode of variation in boreal summer for (a) surface PV over the TP; (b) precipitation over East Asia; and (c) circulation over East Asia at 200 hPa. (d) Corresponding normalized principal components of the first EOF mode are shown in (a), (b), and (c). The blue line in (a), (c) denotes the TP topographic boundary of 2000 m.

two areas are opposite, the southern area is quite small. In general, the distribution of EOF1 on surface PV shows a negative uniform mode (PVNUM). The corresponding normalized first principal component of the EOF pattern (PC1) is defined as the surface PV index (PVS<sub>I</sub>; red line), as shown in Fig. 1d. The variance percentage explained by the first leading mode is 36%.

Figure 1b shows the EOF1 of EASR. The corresponding normalized PC1 is defined as the precipitation index (PreI; blue dashed line), as shown in Fig. 1d. The maximum variation center of EASR occurs in the Yangtze River valley, South Korea, Japan (YKJ), and southern China. The variation in EASR in YKJ has the opposite sign to that in southern China. There is also a relatively weak dipole variation mode in northern China. The dominant mode of EASR obtained in this study is generally consistent with that obtained by Zuo et al. (2011).

Using the NCEP-NCAR reanalysis over midlatitude Asia in JJAS (i.e., June, July, August, and September) from 1948 to 1998, Wu (2002) identified an interannual dominant pattern in the upper-level winds called the midlatitude Asian summer (MAS) pattern. The MAS pattern in his study features two anomalous cyclones, with one centered at (37.5°N, 65°E) and the other centered at (42.5°N, 130°E). Following Wu (2002), we applied MVEOF analysis to the 200-hPa wind anomaly to reveal the dominant circulation mode over midlatitude Asia during boreal summer. The domain for the MVEOF analysis is (20°–60°N, 50°–150°E), and the result is not sensitive to the domain. The first leading mode of MVEOF (MVEOF1) is shown in Fig. 1c, and the corresponding normalized PC1 is defined as the midlatitude Asian summer index (MASI; black dashed line) shown in Fig. 1d. Figure 1c shows two anomalous cyclones, one centered northwest of the TP and one centered over northeastern Asia. In between the two large cyclones is an anticyclone over the southeastern corner of the TP. The anticyclone identified in this study is more prominent than that in Wu (2002), which is partly because of the different reanalysis data and partly because of the different periods. From high to low latitudes, the positive MAS generally shows a “CCA” pattern (i.e., cyclone–cyclone–anticyclone pattern). Correspondingly, the negative MAS generally shows an “AAC” pattern (i.e., anticyclone–anticyclone–cyclone pattern).

To investigate the relationship of surface TPPV forcing with the EASR and upper-level circulation over East Asia, Fig. 1d shows the time series of PVS<sub>I</sub>, MASI, and PreI. PVS<sub>I</sub> shows significant correlations with PreI and MASI, with yield correlation coefficients of 0.56 and 0.74 (both passing the 0.05 significance level), respectively. These results indicate that the EASR and the leading mode of circulation (i.e., MAS pattern) over East Asia are closely related to the surface TPPV forcing.

### 3.2. Relationship of surface TPPV forcing with EASR and associated circulation

Figure 2 shows the spatial pattern of the correlation coef-

ficients between the PVS<sub>I</sub> and EASR anomalies. The pattern (Fig. 2) is similar to EOF1 of EASR (Fig. 1b). A negative correlation appears in southern China, whereas positive correlations are observed in YKJ. A positive correlation, but with a small area, appears in part of northern China. The correlation coefficients in these regions are significant at the 0.05 significance level. A weak negative correlation is seen in the area south of northern China (approximately 42°N), but this correlation is not significant. These results indicate that the positive phase of PVNUM is associated with more rainfall in YKJ and part of northern China and less rainfall in southern China, and the negative phase of PVNUM is related to the opposite rainfall pattern.

To understand the comprehensive three-dimensional relationship between surface TPPV forcing and EASR, the correlation patterns between the PVS<sub>I</sub>, PreI, and circulation anomalies at different levels are shown in Fig. 3. Figures 3a–c show correlation coefficients between PVS<sub>I</sub> and circulation at different levels. Corresponding to the positive (negative) PVNUM, at 200 hPa (Fig. 3a), two anomalous cyclones (anticyclones) appear at middle latitudes at approximately 40°N. One center is located northwest of the TP, and the other is located in northeastern China (Fig. 3a). In addition to these two anomalous cyclones (anticyclones), an anomalous anticyclone (cyclone) center appears at the southeastern corner of the TP. This configuration generally shows the MAS pattern (Fig. 1b). Except for the anomalous cyclone (anticyclone) over the northwestern TP at 850 hPa (Fig. 3c), this equivalent barotropic pattern can also be seen at the middle (Fig. 3b) to lower (Fig. 3c) levels. The correlation between PreI and circulation (Figs. 3d–3f) closely resembles Figs. 3a–c, which further confirms that surface TPPV forcing is significantly related to EASR. In addition, comparing Figs. 3a–c and Figs. 3d–f reveals that the MAS pattern plays an important role in the connection between surface TPPV forcing and EASR.

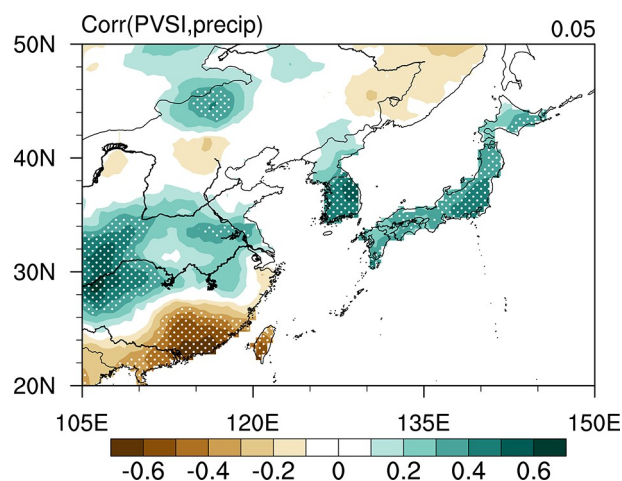
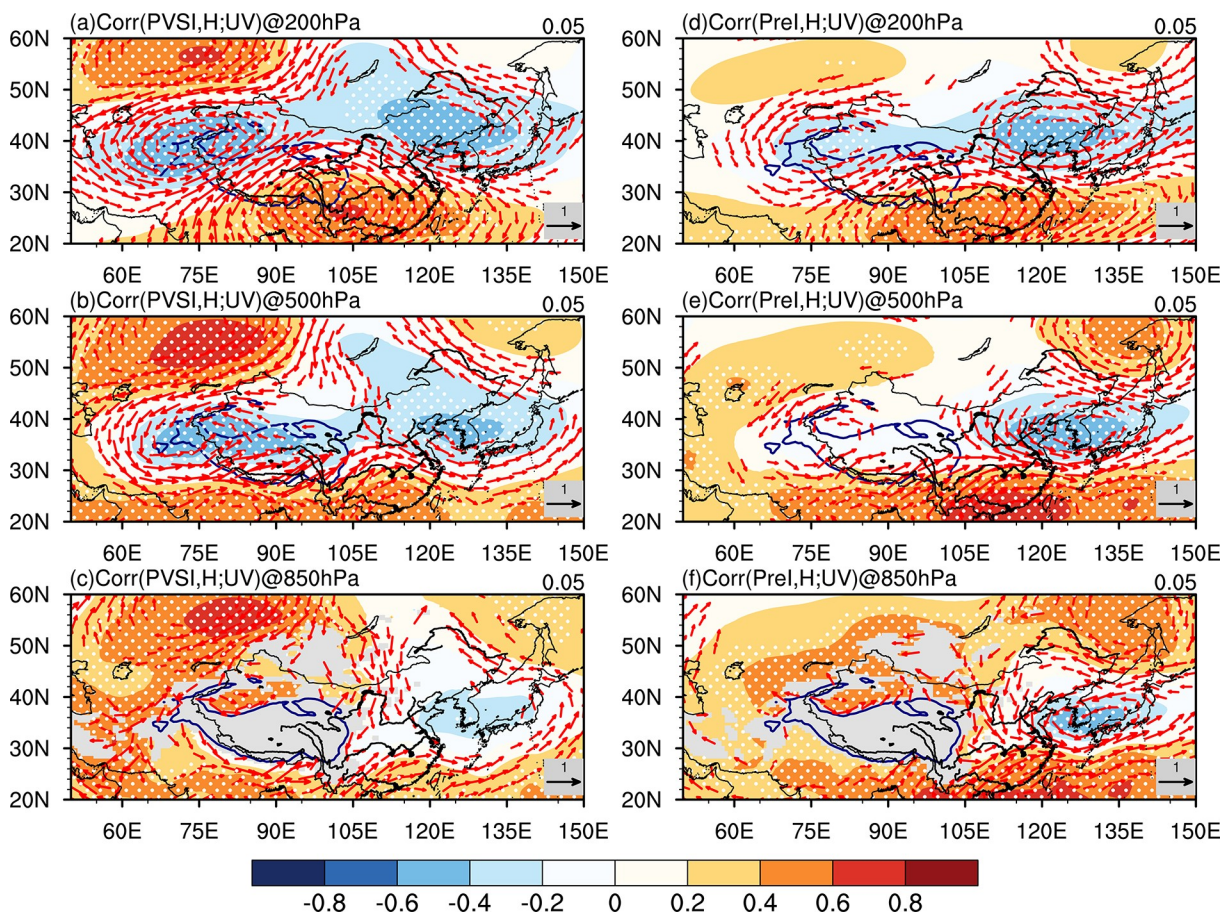


Fig. 2. Spatial distribution of the correlation coefficients between the PVS<sub>I</sub> and downstream rainfall anomalies. Areas exceeding the 0.05 significance level are highlighted with dots.



**Fig. 3.** Spatial distribution of the correlation coefficient between the PVSI and geopotential height anomalies (shading) and circulation anomalies (vector, those passing the 0.05 significance level are shown) at (a) 200 hPa; (b) 500 hPa; and (c) 850 hPa. (d–f) are the same as (a–c), but for PreI. Areas exceeding the 0.05 significance level are highlighted with dots. The blue line denotes the TP topographic boundary of 3000 m.

#### 4. Possible mechanism of the surface TPPV forcing affecting the EASR

To investigate the possible mechanism of surface TPPV forcing affecting EASR, the LBM is employed in this section to examine the response of upper circulation to the anomalous heating related to surface TPPV forcing.

##### 4.1. Diagnostic analysis

Surface PV is closely related to the static stability within the surface layer. Figure 4a shows the correlation coefficient between PVSI and static stability anomalies. The correlation between the PVSI and horizontal wind anomalies at the surface and vertical motion ( $\omega$ ) anomalies at 500 hPa are shown in Fig. 4b. Corresponding to the positive phase of PVNUM, the anomalous static stability over the whole TP is significantly negative (Fig. 4a). This result means that the air within the surface layer over the TP is anomalously statically unstable. As a result, the anomalous  $\omega$  is significantly negative, accompanied by anomalous upward motion occurring at the main body of the TP (Fig. 4b). Consequently, a significant anomalous cyclonic circulation is generated at the surface south of the TP (Fig. 4b).

The negative phase of PVNUM corresponds to the opposite situation of surface static stability and circulation pattern.

The anomalous south and north winds associated with the anomalous circulation to the south of the TP (Fig. 4b) induced by surface TPPV forcing could lead to anomalous heating over the TP. Figure 5 shows the correlation coefficient between PVSI and OLR (Fig. 5a) and regressed rainfall anomalies against PVSI (Fig. 5b) to examine the distribution of anomalous heating. A dipole mode of the OLR anomalies is clearly observed in Fig. 5a. Corresponding to the positive phase of PVNUM, positive OLR anomalies cover the southwestern TP to northern India. The highest negative OLR anomalies mainly occur on the eastern TP, whereas the highest positive OLR anomalies mainly occur on the western TP. The anomalous cyclonic circulation (Fig. 4b), with cool and divergent flow to its western part and wet, warm flow to its eastern part, accounts for this clear dipole mode of the OLR (Fig. 5a). Consistent with the OLR, the rainfall anomalies also show a dipole mode (Fig. 5b) with less rainfall over the southwestern TP and northern India and more rainfall over the eastern TP. The rainfall anomalies indicate that the strongest negative and positive condensational heating anomalies occur at the southwestern TP to northern

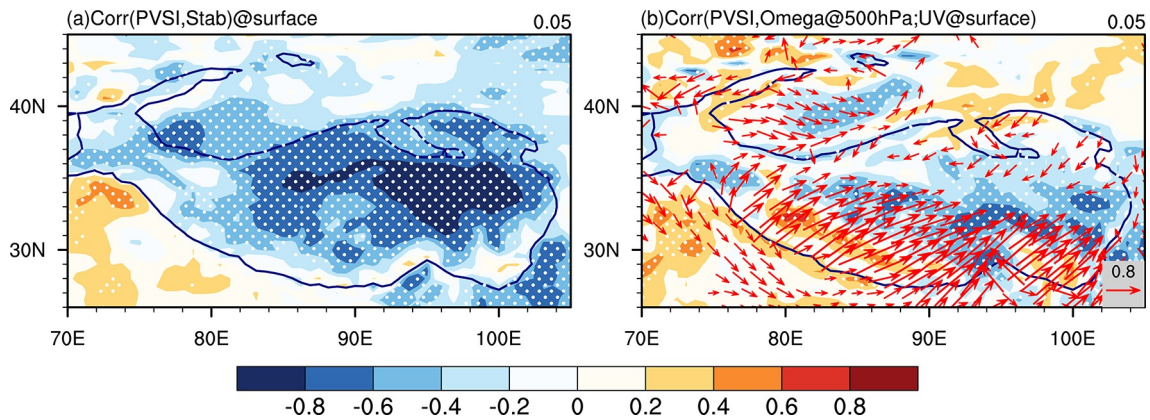


**Fig. 4.** Spatial distribution of the correlation coefficient between the PVSI and (a) surface static stability anomalies and (b) horizontal wind anomalies at the surface (vector, those exceeding the 0.05 significance test are shown) and  $\omega$  at 500 hPa (shading). Areas exceeding the 0.05 significance level are highlighted with dots. The blue line denotes the TP topographic boundary of 3000 m.

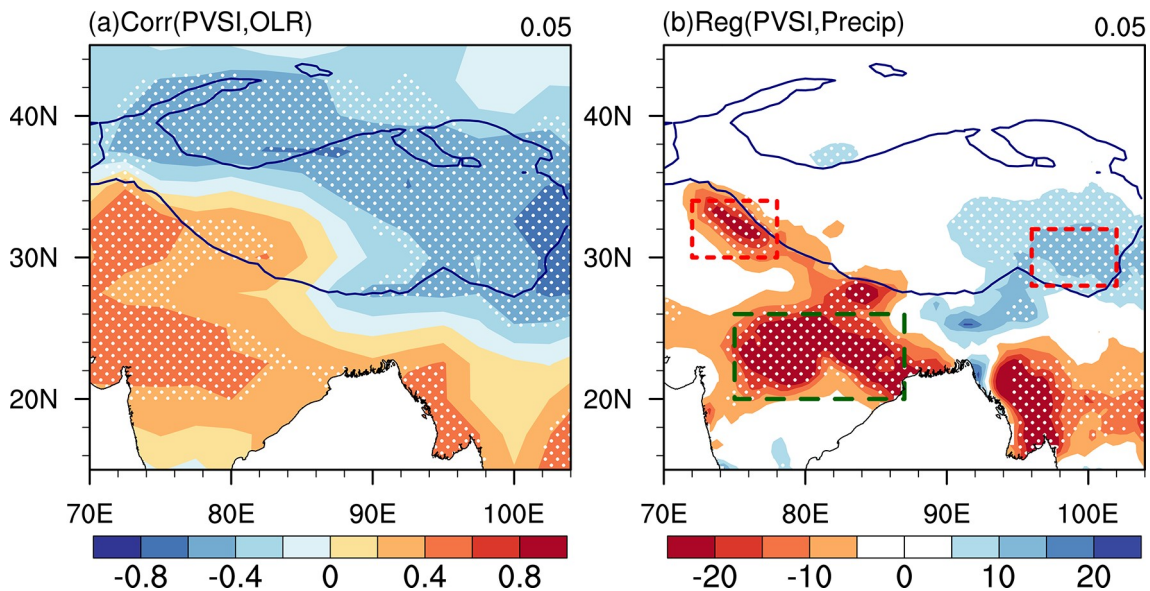


**Fig. 5.** Spatial distribution of the (a) correlation coefficient between the PVSI and OLR anomalies and (b) regressed rainfall anomalies against the PVSI (units:  $\text{mm month}^{-1}$ ). Areas exceeding the 0.05 significance level are highlighted with dots. The blue line denotes the TP topographic boundary of 3000 m.

India and the eastern TP, respectively. Corresponding to the negative phase of PVNUM, the situation is opposite.

**4.2. Sensitivity experiments**

The response of upper-level circulation to the negative heating anomaly over northern India has been examined in Wei et al. (2014). Because the lower latitude of the negative heating anomaly over northern India (Fig. 5b) is far away from the westerly jet (light green shading in Fig. 7) at high latitudes in the north, the associated atmospheric response regarding the negative heating anomaly over northern India is trapped south of 40°N (Wei et al., 2014; see their Fig. 8), exhibiting a zonal dipole mode with an anomalous cyclone to the west of 80°E and an anomalous anticyclone to the east of 80°E. There are some differences between the circulation caused by the negative heating anom-

ally over northern India (Wei et al., 2014; see their Fig. 8) and the MAS pattern (Fig. 3) related to EASR. Hence, regarding the negative heating centered on the southwestern TP and northern India, we focus on the southwestern TP in this study.

Based on the diagnostic analysis of heating anomalies induced by surface TPPV forcing, three groups of experiments are conducted. Expt1 is an experiment of positive heating over the southeastern TP (Expt1, Figs. 6a–b). Expt2 is an experiment of negative heating over the southwestern TP (Expt2, Figs. 6c–d). Expt3 is an experiment of combined positive and negative heating over the southeastern and southwestern TP, respectively (Expt3, Fig. 6e). According to the reanalysis, the heating centers are at 30°N, 99°E and 32°N, 75°E in Expt1 and Expt2, respectively. The peaks of the ideal heating profiles in Expt1 and Expt2 are 1.0 K d<sup>-1</sup> and

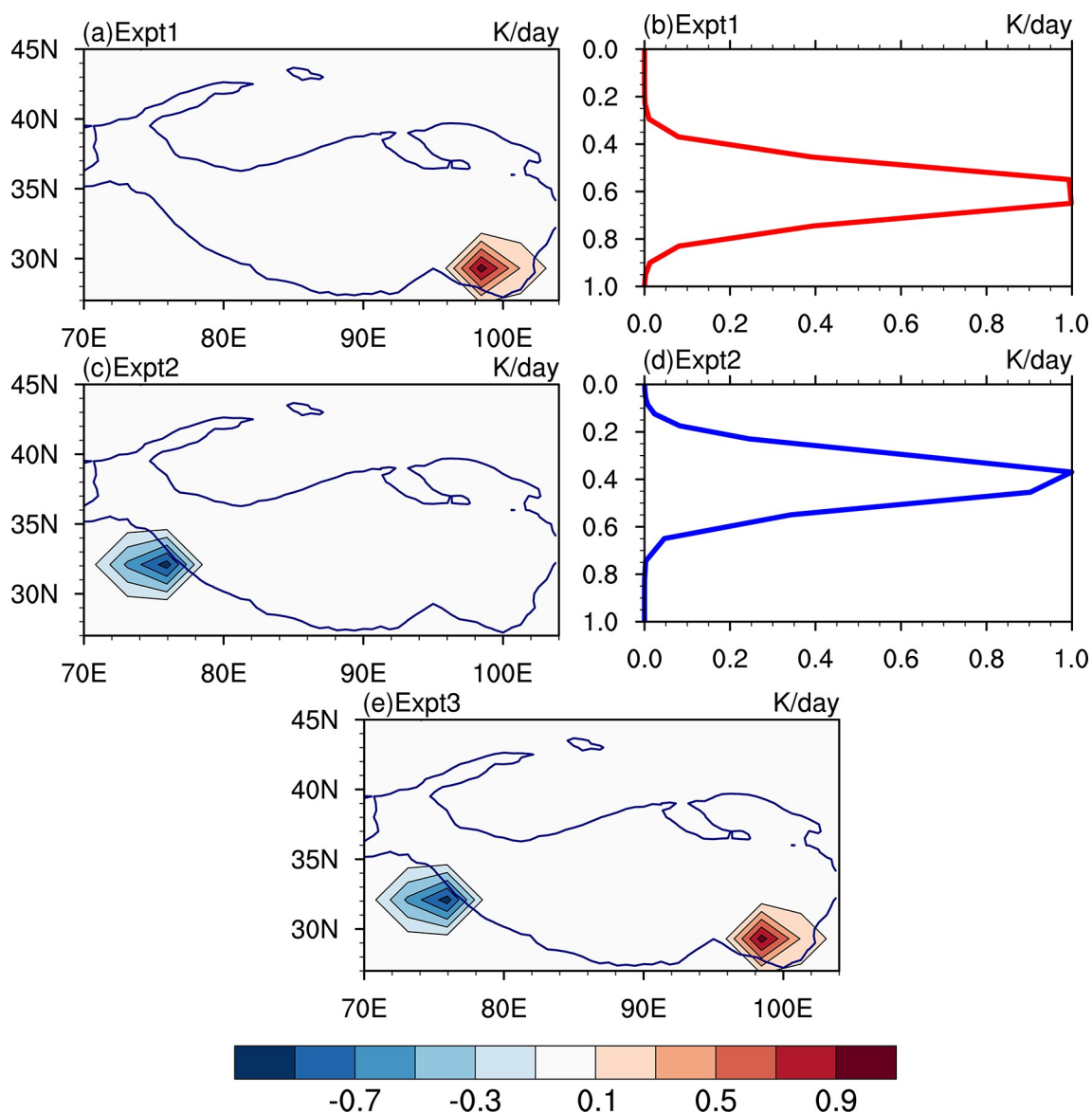


**Fig. 6.** Specified ideal diabatic heating (units:  $\text{K d}^{-1}$ ) horizontal distribution in (a) Expt1; (c) Expt2; and (e) Expt3. Specified ideal diabatic heating (units:  $\text{K d}^{-1}$ ) profiles in (b) Expt1 and (d) Expt2. The blue line denotes the TP topographic boundary of 3000 m.

$-1.0 \text{ K d}^{-1}$ , respectively. The peaks in the heating profile are at  $\sigma=0.6$  and  $\sigma=0.4$  in Expt1 and Expt2, respectively. Since the LBM is a linear model, the heating configuration (Fig. 6e) and atmospheric response (Fig. 7c) in Expt3 are linear combinations of Expt1 and Expt2.

The atmospheric responses are shown in Fig. 7. In Expt1 (Fig. 7a), the positive heating anomaly over the eastern TP triggers a local anomalous anticyclone and high height at 200 hPa. The anomalous high is strengthened locally with slight northward and westward dispersion. In Expt2 (Fig. 7b), the negative heating anomaly over the southwestern TP stimulates a local anomalous cyclone and low height at 200 hPa. Compared with Wei et al. (2014), because the location of the negative heating center over the southwestern TP is farther north than that over northern India, the anomalous cyclone could trigger waves in the west-

erly jet and lead to an anomalous cyclone downstream over northeastern China. In Expt3 (Fig. 7c), the response of atmospheric circulation with the “CCA” pattern is very similar to the MAS pattern related to EASR (Figs. 3d–f). These results indicate that the dipole heating mode induced by surface TPPV forcing can lead to a realistic MAS pattern, which is important for the formation of the anomalous EASR.

### 4.3. Influence of circulation anomalies on EASR

The above results indicate that surface TPPV forcing can lead to the formation of the MAS pattern. In this section, we examine how the MAS pattern affects the EASR anomalies.

Rainfall anomalies are related to water vapor transport anomalies and their divergence at the lower level. Since atmo-

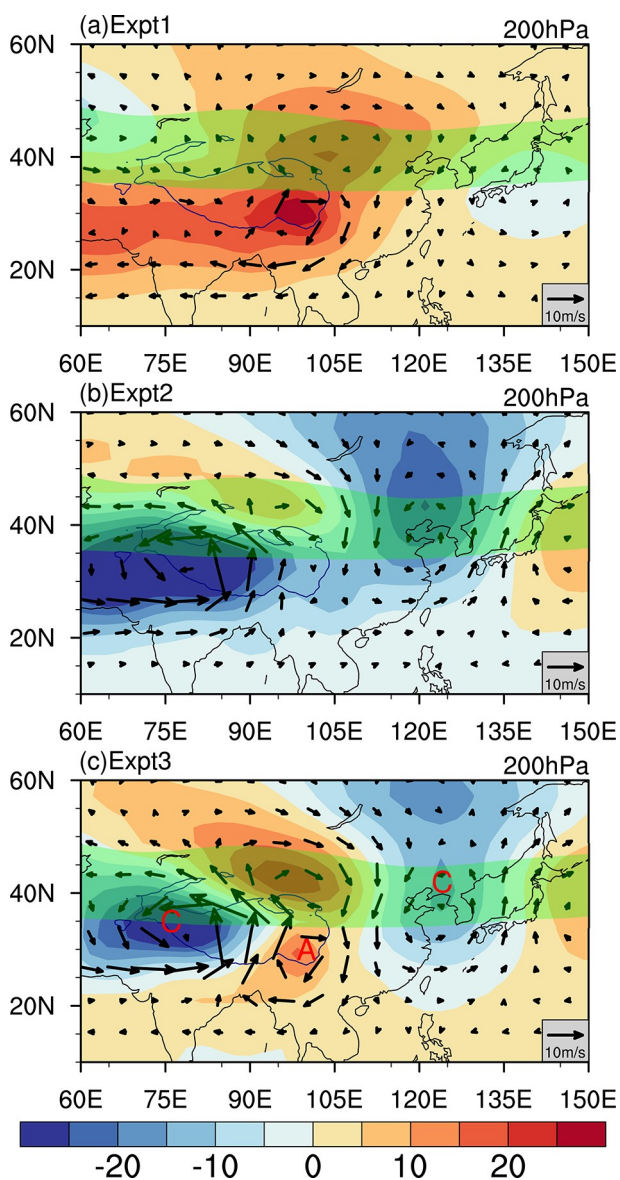


**Fig. 7.** Responses of geopotential height (shading, units: gpm) and horizontal wind (vector, units:  $m s^{-1}$ ) at 200 hPa in (a) Expt1; (b) Expt2; and (c) Expt3. The blue line denotes the TP topographic boundary of 3000 m. The light green shading indicates a westerly jet with a zonal wind speed greater than  $20 m s^{-1}$  at 200 hPa. The “A” and “C” in Fig. 7c indicate the anomalous anticyclone and cyclone, respectively.

spheric moisture is mainly concentrated at the middle to lower levels, Fig. 8 shows the correlation between PVSI and WVF and its divergence at 500 hPa (Fig. 8a) and 850 hPa (Fig. 8b). Generally, the anomalous WVF (Fig. 8) shows an equivalent barotropic structure. This equivalent barotropic structure markedly resembles the MAS pattern. Corresponding to the positive phase of PVNUM, the anomalous cyclonic WVF (Fig. 8) over northeastern China embedded in the MAS pattern converges water vapor over South Korea and Japan and, cooperating with the southern anticyclonic WVF, converges the wet, warm southwesterly flow and dry, cold northerly wind to the Yangtze River valley. In addition,

an anomalous convergence of WVF (Fig. 8) occurs in part of northern China. Hence, the EASR over YKJ and part of northern China is greater than normal (Fig. 2). Although the WVF transfers water vapor to southern China, the WVF is divergent. Thus, the EASR over southern China is lower than normal (Fig. 2). Corresponding to the negative phase of PVNUM, the situation is opposite. These results indicate that the WVF anomalies related to the MAS pattern are responsible for the EASR anomalies.

### 5. Conclusion and discussion

The present study investigates the relationship between the surface PV forcing over the TP and EASR and the associated circulation on the interannual timescale and the possible mechanism. The main conclusions obtained from the results are described as follows.

The correlation between the time series of the leading mode of the surface PV forcing over the TP (i.e., PVNUM) and EASR and the leading mode of upper-level circulation (i.e., MAS pattern) are as high as 0.56 and 0.74, respectively. Moreover, the circulation related to PVNUM greatly resembles the circulation associated with EASR. These results indicated that the interannual EASR and related upper-level circulation over East Asia are closely linked to the surface PV forcing over the TP, and the MAS pattern plays an important role in the PVNUM affecting EASR. Diagnostic analysis indicates that the positive phase of PVNUM could lead to unstable air within the surface layer over the TP. As a result, anomalous upward motion and cyclonic circulation are generated over the TP. Induced by cyclonic circulation, a dipole heating mode with anomalous cooling over the southwestern TP and anomalous heating over the southeastern TP appeared. Sensitivity experiments prove that the dipole heating mode associated with the surface PV forcing over the TP can trigger the MAS pattern related to EASR anomalies. The MAS pattern converges water vapor to the Yangtze River valley, South Korea, Japan, and part of northern China and diverges water vapor over southern China. Therefore, the EASR over the Yangtze River valley, South Korea, Japan, and part of northern China is greater than normal, and that over southern China is lower. The negative phase of PVNUM is related to the opposite rainfall and circulation pattern. Consequently, the surface PV forcing over the TP exerts a significant influence on EASR by changing the air static stability within the surface layer over the TP and causing the dipole heating mode and the subsequent anomalous water vapor transport related to the MAS pattern.

The aforementioned major mechanism is briefly shown schematically in Fig. 9. In summary, PVNUM triggers lower-level cyclonic circulation by reducing the surface static stability (Fig. 9b). The dipole heating mode induced by this cyclonic circulation could lead to anomalous circulation at the upper level (Fig. 9a). As a result, the anomalous water vapor transport (Fig. 8) embedded in the upper-level anomalous circulation is responsible for EASR anomalies



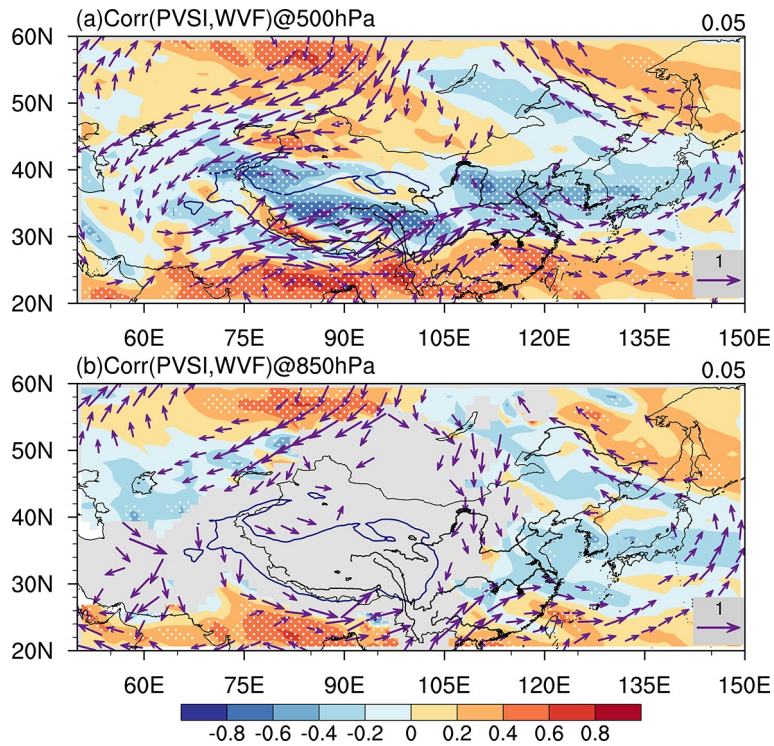


**Fig. 8.** Spatial distribution of the correlation coefficient between the PVSI and the divergence of WVF anomalies (shading) and WVF anomalies (vector, those passing the 0.05 significance level are shown) at (a) 500 hPa and (b) 850 hPa. Areas exceeding the 0.05 significance level are highlighted with dots. The blue line denotes the TP topographic boundary of 3000 m.

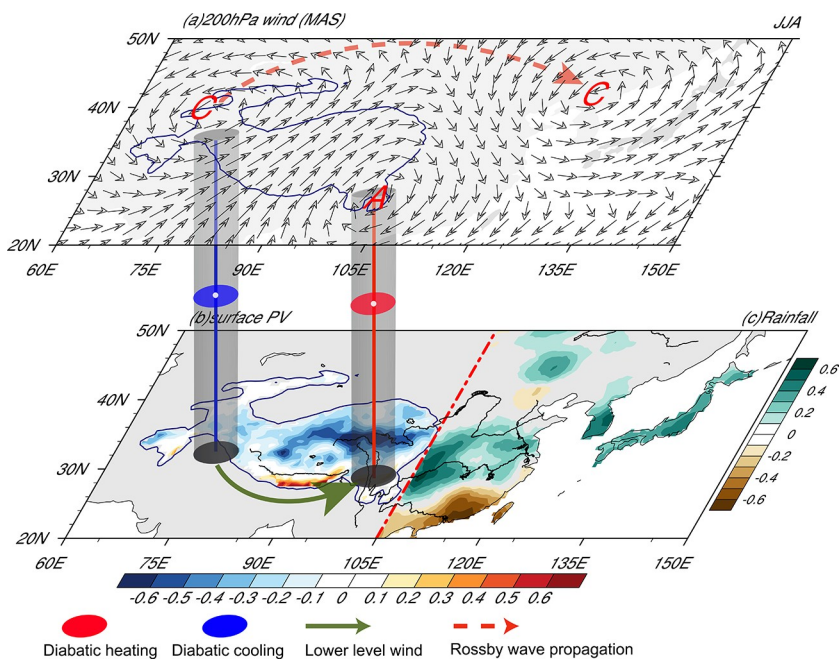


**Fig. 9.** Schematic showing the interannual surface TPPV influence on EASR. (a) Anomalous 200-hPa wind associated with surface TPPV forcing; (b) anomalous surface TPPV; and (c) same as (a) but for rainfall anomalies. The red (blue) circle indicates diabatic heating (cooling). The green (red) vector indicates the lower-level wind (upper-level Rossby wave propagation).

(Fig. 9c).

Previous studies (e.g., Wu, 2002) show that the MAS pattern is related to the Indian summer monsoon. We calculated the concurrent correlation coefficient between the MASI and Indian summer monsoon index (defined by Wang et al., 2001) and found that the correlation coefficient reaches  $-0.45$ , passing the 0.05 significance test; however, when the index of the surface TPPV forcing (i.e., PVSJ, red line in Fig. 1d) is removed, it is reduced to  $-0.28$ , which does not pass the significance test. This result further confirms the important role of surface TPPV forcing on EASR. ENSO is the most prominent interannual signal in climate systems. We also calculated the correlation between the summer PVSJ and NINO3.4 index (SST averaged over the region  $5^{\circ}\text{S}$ – $5^{\circ}\text{N}$ ,  $170^{\circ}$ – $120^{\circ}\text{W}$ ; <https://psl.noaa.gov/data/climateindices/list/>) in the preceding winter and concurrent summer. The coefficients are 0.21 and  $-0.18$ , respectively, which do not pass the significance test, meaning that the relationship between surface TPPV forcing and EASR is unaffected by ENSO. It should be noted that some studies (e.g., Guan et al., 2015) suggested that North Atlantic Oscillation, Pacific Decadal Oscillation, and Atlantic Multidecadal Oscillation have great impact on surface air temperature, which is related to surface PV. The role of these decadal oscillations in the interdecadal variation of surface TPPV will be investigated in the future.

The present study only focuses on the impacts of the TP on monsoon rainfall over East Asia. The complicated Asian summer monsoon system, greatly affected by the TP, includes the South Asian summer monsoon and the East Asian summer monsoon. Research on the relationship between the PV anomaly over the TP and monsoon rainfall, as well as wind fields over the Asian region will be conducted in the future. In this study, although the simple model (e.g., LBM) clearly shows the impact of surface TPPV forcing on EASR, it is still necessary to use a fully coupled model to examine the surface TPPV–rainfall–circulation feedback to understand the interactions between the surface TP forcing and EASM system. Furthermore, with the help of the PV budget equation, the relative importance of dynamic PV advection, PV generation due to diabatic heating, and friction effects to the variation of surface PV will be quantitatively answered, which will greatly advance our understanding of the TP's impacts.

**Acknowledgements.** We thank the reviewers for their constructive suggestions and comments. This work is jointly supported by the National Natural Science Foundation of China (Grant Nos. 91837101, 42122035, and 91937302) and the National Key Research and Development Program of China (Grant No. 2018YFC1505706 and 2020YFA0608903).

**Open Access** This article is distributed under the terms of the Creative Commons Attribution 4.0 International License (<http://creativecommons.org/licenses/by/4.0/>), which permits unrestricted use, distribution, and reproduction in any medium, provided you give appropriate credit to the original author(s) and the source,

provide a link to the Creative Commons license, and indicate if changes were made.

## REFERENCES

- Allaart, M. A. F., H. Kelder, and L. C. Heijboer, 1993: On the Relation between Ozone and Potential Vorticity. *Geophys. Res. Lett.*, **20**, 811–814, <https://doi.org/10.1029/93GL00822>.
- Bowley, K. A., J. R. Gyakum, and E. H. Atallah, 2019: A new perspective toward cataloging northern hemisphere rossby wave breaking on the dynamic tropopause. *Mon. Wea. Rev.*, **147**, 409–431, <https://doi.org/10.1175/MWR-D-18-0131.1>.
- Chen, L. X., J. P. Liu, X. J. Zhou, and P. X. Wang, 1999: Impact of uplift of Qinghai-Xizang Plateau and change of land-ocean distribution on climate over Asia. *Quaternary Sciences*, 314–329. (in Chinese with English abstract)
- Danielsen, E. F., 1968: Stratospheric-tropospheric exchange based on radioactivity, ozone and potential vorticity. *J. Atmos. Sci.*, **25**, 502–518, [https://doi.org/10.1175/1520-0469\(1968\)025<0502:STEBOR>2.0.CO;2](https://doi.org/10.1175/1520-0469(1968)025<0502:STEBOR>2.0.CO;2).
- Ding, Y. H., 2007: The variability of the Asian summer monsoon. *J. Meteor. Soc. Japan*, **85B**, 21–54, <https://doi.org/10.2151/jmsj.85B.21>.
- Ding, Y. H., and J. C. L. Chan, 2005: The East Asian summer monsoon: An overview. *Meteor. Atmos. Phys.*, **89**, 117–142, <https://doi.org/10.1007/s00703-005-0125-z>.
- Ding, Y. H., P. Liang, Y. J. Liu, and Y. C. Zhang, 2020: Multiscale variability of meiyy and its prediction: A new review. *J. Geophys. Res.*, **125**, e2019JD031496, <https://doi.org/10.1029/2019JD031496>.
- Duan, A. M., Y. M. Liu, and G. X. Wu, 2005: Heating status of the Tibetan Plateau from april to june and rainfall and atmospheric circulation anomaly over East Asia in midsummer. *Science in China Series D: Earth Sciences*, **48**, 250–257, <https://doi.org/10.1360/02yd0510>.
- Ertel, H., 1942: Ein neuer hydrodynamischer wirbelsatz. *Meteorologische Zeitschrift*, **59**, 271–281.
- Flohn, H., 1957: Large-scale aspects of the “Summer Monsoon” in South and East Asia. *J. Meteor. Soc. Japan*, **35A**, 180–186, [https://doi.org/10.2151/jmsj1923.35A.0\\_180](https://doi.org/10.2151/jmsj1923.35A.0_180).
- Folkens, I., and C. Appenzeller, 1996: Ozone and potential vorticity at the subtropical tropopause break. *J. Geophys. Res.*, **101**, 18787–18792, <https://doi.org/10.1029/96JD01711>.
- Guan, X. D., J. P. Huang, R. X. Guo, and P. Lin, 2015: The role of dynamically induced variability in the recent warming trend slowdown over the Northern Hemisphere. *Scientific Reports*, **5**, 12669, <https://doi.org/10.1038/srep12669>.
- Hahn, D. G., and S. Manabe, 1975: The role of mountains in the South Asian monsoon circulation. *J. Atmos. Sci.*, **32**, 1515–1541, [https://doi.org/10.1175/1520-0469\(1975\)032<1515:TROMIT>2.0.CO;2](https://doi.org/10.1175/1520-0469(1975)032<1515:TROMIT>2.0.CO;2).
- Haynes, P. H., and M. E. McIntyre, 1987: On the evolution of vorticity and potential vorticity in the presence of diabatic heating and frictional or other forces. *J. Atmos. Sci.*, **44**, 828–841, [https://doi.org/10.1175/1520-0469\(1987\)044<0828:OTEOVA>2.0.CO;2](https://doi.org/10.1175/1520-0469(1987)044<0828:OTEOVA>2.0.CO;2).
- Haynes, P. H., and M. E. McIntyre, 1990: On the conservation and impermeability theorems for potential vorticity. *J. Atmos. Sci.*, **47**, 2021–2031, [https://doi.org/10.1175/1520-0469\(1990\)047<2021:OTCAIT>2.0.CO;2](https://doi.org/10.1175/1520-0469(1990)047<2021:OTCAIT>2.0.CO;2).
- Hoskins, B. J., 1991: Towards a PV- $\theta$  view of the general circula-

- tion. *Tellus A*, **43**, 27–36, <https://doi.org/10.3402/tellusa.v43i4.11936>.
- Hsu, H.-H., and X. Liu, 2003: Relationship between the Tibetan Plateau heating and East Asian summer monsoon rainfall. *Geophys. Res. Lett.*, **30**, 2066, <https://doi.org/10.1029/2003GL017909>.
- Huang, J. P., W. Chen, Z. P. Wen, G. J. Zhang, Z. X. Li, Z. Y. Zuo, and Q. Y. Zhao, 2019: Review of Chinese atmospheric science research over the Past 70 Years: Climate and climate change. *Science China Earth Sciences*, **62**, 1514–1550, <https://doi.org/10.1007/s11430-019-9483-5>.
- Huang, R. H., J. L. Chen, and G. Huang, 2007: Characteristics and variations of the East Asian monsoon system and its impacts on climate disasters in China. *Adv. Atmos. Sci.*, **24**, 993–1023, <https://doi.org/10.1007/s00376-007-0993-x>.
- Jiang, D. B., Z. L. Ding, H. Drange, and Y. Q. Gao, 2008: Sensitivity of East Asian climate to the progressive uplift and expansion of the Tibetan Plateau under the Mid-pliocene boundary conditions. *Adv. Atmos. Sci.*, **25**, 709–722, <https://doi.org/10.1007/s00376-008-0709-x>.
- Kitoh, A., 2004: Effects of mountain uplift on East Asian summer climate investigated by a coupled atmosphere-ocean GCM. *J. Climate*, **17**, 783–802, [https://doi.org/10.1175/1520-0442\(2004\)017<0783:EOMUOE>2.0.CO;2](https://doi.org/10.1175/1520-0442(2004)017<0783:EOMUOE>2.0.CO;2).
- Kripalani, R. H., and A. Kulkarni, 1997: Climatic impact of El Niño/La Niña on the Indian Monsoon: A new perspective. *Weather*, **52**, 39–46, <https://doi.org/10.1002/j.1477-8696.1997.tb06267.x>.
- Kripalani, R. H., and A. Kulkarni, 2001: Monsoon rainfall variations and teleconnections over South and East Asia. *International Journal of Climatology*, **21**, 603–616, <https://doi.org/10.1002/joc.625>.
- Kubota, H., Y. Kosaka, and S.-P. Xie, 2016: A 117-year long index of the Pacific-Japan pattern with application to interdecadal variability. *International Journal of Climatology*, **36**, 1575–1589, <https://doi.org/10.1002/joc.4441>.
- Liang, X. Y., Y. M. Liu, and G. X. Wu, 2005: Effect of Tibetan Plateau on the site of onset and intensity of the Asian summer monsoon. *Acta Meteorologica Sinica*, **63**, 799–805, <https://doi.org/10.3321/j.issn:0577-6619.2005.05.023>. (in Chinese with English abstract)
- Liebmann, B., and C. A. Smith, 1996: Description of a complete (interpolated) outgoing longwave radiation dataset. *Bull. Amer. Meteor. Soc.*, **77**, 1275–1277.
- Liu, X.-D., 1999: Influences of Qinghai-Xizang (Tibet) Plateau uplift on the atmospheric circulation, global climate and environment changes. *Plateau Meteorology*, **18**, 321–332, <https://doi.org/10.3321/j.issn:1000-0534.1999.03.008>. (in Chinese with English abstract)
- Liu, X. D., and Z.-Y. Yin, 2002: Sensitivity of East Asian monsoon climate to the uplift of the Tibetan Plateau. *Palaeogeography, Palaeoclimatology, Palaeoecology*, **183**, 223–245, [https://doi.org/10.1016/S0031-0182\(01\)00488-6](https://doi.org/10.1016/S0031-0182(01)00488-6).
- Liu, Y. M., M. M. Lu, H. J. Yang, A. M. Duan, B. He, S. Yang, and G. X. Wu, 2020: Land-atmosphere-ocean coupling associated with the Tibetan Plateau and its climate impacts. *National Science Review*, **7**, 534–552, <https://doi.org/10.1093/nsr/nwaa011>.
- Lucchini, R., 2012: File specification for merra products. Gmao Office Note No.1 (Version 2.3), 87 pp. Available from <https://gmao.gsfc.nasa.gov/pubs/docs/lucchini528.pdf>.
- Ma, T. T., G. X. Wu, Y. M. Liu, Z. H. Jiang, and J. H. Yu, 2019: Impact of surface potential vorticity density forcing over the Tibetan Plateau on the South China extreme precipitation in January 2008. *Part I: Data analysis. Journal of Meteorological Research*, **33**, 400–415, <https://doi.org/10.1007/s13351-019-8604-1>.
- Mitchell, T. D., and P. D. Jones, 2005: An improved method of constructing a database of monthly climate observations and associated high-resolution grids. *International Journal of Climatology*, **25**, 693–712, <https://doi.org/10.1002/joc.1181>.
- Rienecker, M. M., and Coauthors, 2011: MERRA: NASA's modern-era retrospective analysis for research and applications. *J. Climate*, **24**, 3624–3648, <https://doi.org/10.1175/JCLI-D-11-00015.1>.
- Rosby, C.-G., 1940: Planetary flow patterns in the atmosphere. *Quart. J. Roy. Meteor. Soc.*, **66**, 68–87.
- Ryoo, J.-M., Y. Kaspi, D. W. Waugh, G. N. Kiladis, D. E. Waliser, E. J. Fetzer, and J. Kim, 2013: Impact of rossby wave breaking on U. S. west coast winter precipitation during enso events. *J. Climate*, **26**, 6360–6382, <https://doi.org/10.1175/JCLI-D-12-00297.1>.
- Sandhya, M., S. Sridharan, M. I. Devi, and H. Gadhavi, 2015: Tropical upper tropospheric ozone enhancements due to potential vorticity intrusions over Indian sector. *Journal of Atmospheric and Solar-Terrestrial Physics*, **132**, 147–152, <https://doi.org/10.1016/j.jastp.2015.07.014>.
- Sheng, C., and Coauthors, 2021: Characteristics of the potential vorticity and its budget in the surface layer over the Tibetan Plateau. *International Journal of Climatology*, **41**, 439–455, <https://doi.org/10.1002/joc.6629>.
- Wang, B., and Q. Zhang, 2002: Pacific-East Asian teleconnection. Part II: How the philippine sea anomalous anticyclone is established during El Niño development. *J. Climate*, **15**, 3252–3265, [https://doi.org/10.1175/1520-0442\(2002\)015<3252:PEATPI>2.0.CO;2](https://doi.org/10.1175/1520-0442(2002)015<3252:PEATPI>2.0.CO;2).
- Wang, B., R. G. Wu, and K.-M. Lau, 2001: Interannual variability of the Asian summer monsoon: Contrasts between the indian and the western North Pacific-East Asian monsoons. *J. Climate*, **14**, 4073–4090, [https://doi.org/10.1175/1520-0442\(2001\)014<4073:IVOTAS>2.0.CO;2](https://doi.org/10.1175/1520-0442(2001)014<4073:IVOTAS>2.0.CO;2).
- Watanabe, M., and M. Kimoto, 2000: Atmosphere-ocean thermal coupling in the North Atlantic: A positive feedback. *Quart. J. Roy. Meteor. Soc.*, **126**, 3343–3369, <https://doi.org/10.1002/qj.49712657017>.
- Watanabe, M., and F.-F. Jin, 2003: A moist linear baroclinic model: Coupled dynamical-convective response to El Niño. *J. Climate*, **16**, 1121–1139, [https://doi.org/10.1175/1520-0442\(2003\)16<1121:AMLBMC>2.0.CO;2](https://doi.org/10.1175/1520-0442(2003)16<1121:AMLBMC>2.0.CO;2).
- Watanabe, M., M. Kimoto, T. Nitta, and M. Kachi, 1999: A comparison of decadal climate oscillations in the North Atlantic detected in observations and a coupled GCM. *J. Climate*, **12**, 2920–2940, [https://doi.org/10.1175/1520-0442\(1999\)012<2920:ACODCO>2.0.CO;2](https://doi.org/10.1175/1520-0442(1999)012<2920:ACODCO>2.0.CO;2).
- Wei, W., R. H. Zhang, M. Wen, X. Y. Rong, and T. Li, 2014: Impact of Indian summer monsoon on the South Asian high and its influence on summer rainfall over China. *Climate Dyn.*, **43**, 1257–1269, <https://doi.org/10.1007/s00382-013-1938-y>.
- Wen, N., Z. Y. Liu, and L. Li, 2019: Direct ENSO impact on East Asian summer precipitation in the developing summer. *Climate Dyn.*, **52**, 6799–6815, <https://doi.org/10.1007/s00382-018-4545-0>.
- Wu, G. X., and Y. P. Cai, 1997: Vertical wind shear and down-slid-

- ing slantwise vorticity development. *Scientia Atmospherica Sinica*, **21**, 273–282, <https://doi.org/10.3878/j.issn.1006-9895.1997.03.03>. (in Chinese with English abstract)
- Wu, G. X., and Y. S. Zhang, 1998: Tibetan Plateau forcing and the timing of the monsoon onset over South Asia and the South China Sea. *Mon. Wea. Rev.*, **126**, 913–927, [https://doi.org/10.1175/1520-0493\(1998\)126<0913:TPFATT>2.0.CO;2](https://doi.org/10.1175/1520-0493(1998)126<0913:TPFATT>2.0.CO;2).
- Wu, G. X., Y. P. Cai, and X. J. Tang, 1995: Moist potential vorticity and slantwise vorticity development. *Acta Meteorologica Sinica*, **53**, 387–405, <https://doi.org/10.11676/qxxb1995.045>. (in Chinese with English abstract)
- Wu, G. X., W. J. Li, and H. Guo, 1997: Sensible heat driven air-pump over the Tibetan Plateau and its impacts on the Asian Summer monsoon. *Collections on the Memory of Zhao Jiuzhang*, D. Z. Ye, Ed., Science Press, 116–126. (in Chinese)
- Wu, G. X., and Coauthors, 2007: The influence of mechanical and thermal forcing by the Tibetan Plateau on Asian Climate. *Journal of Hydrometeorology*, **8**, 770–789, <https://doi.org/10.1175/JHM609.1>.
- Wu, G. X., Y. M. Liu, B. W. Dong, X. Y. Liang, A. M. Duan, Q. Bao, and J. J. Yu, 2012: Revisiting Asian monsoon formation and change associated with Tibetan Plateau forcing: I. Formation. *Climate Dyn.*, **39**, 1169–1181, <https://doi.org/10.1007/s00382-012-1334-z>.
- Wu, G. X., Y. M. Liu, B. He, Q. Bao, and Z. Q. Wang, 2018: Review of the impact of the Tibetan Plateau sensible heat driven air-pump on the Asian summer monsoon. *Chinese Journal of Atmospheric Sciences*, **42**, 488–504, <https://doi.org/10.3878/j.issn.1006-9895.1801.17279>.
- Wu, R. G., 2002: A Mid-Latitude Asian circulation anomaly pattern in boreal summer and its connection with the Indian and East Asian summer monsoons. *International Journal of Climatology*, **22**, 1879–1895, <https://doi.org/10.1002/joc.845>.
- Xie, S.-P., K. M. Hu, J. Hafner, H. Tokinaga, Y. Du, G. Huang, and T. Sampe, 2009: Indian ocean capacitor effect on Indo-Western pacific climate during the summer following El Niño. *J. Climate*, **22**, 730–747, <https://doi.org/10.1175/2008JCLI2544.1>.
- Xie, S.-P., Y. Kosaka, Y. Du, K. M. Hu, J. S. Chowdary, and G. Huang, 2016: Indo-Western pacific ocean capacitor and coherent climate anomalies in Post-ENSO summer: A review. *Adv. Atmos. Sci.*, **33**, 411–432, <https://doi.org/10.1007/s00376-015-5192-6>.
- Xu, X. D., T. L. Zhao, X. H. Shi, and C. G. Lu, 2015: A study of the role of the Tibetan Plateau's thermal forcing in modulating rainband and moisture transport in Eastern China. *Acta Meteorologica Sinica*, **73**, 20–35, <https://doi.org/10.11676/qxxb2014.051>. (in Chinese with English abstract)
- Yanai, M., C. F. Li, and Z. S. Song, 1992: Seasonal heating of the Tibetan Plateau and its effects on the evolution of the Asian summer monsoon. *J. Meteor. Soc. Japan*, **70**, 319–351, [https://doi.org/10.2151/jmsj1965.70.1B\\_319](https://doi.org/10.2151/jmsj1965.70.1B_319).
- Yang, J. L., Q. Y. Liu, S.-P. Xie, Z. Y. Liu, and L. X. Wu, 2007: Impact of the Indian ocean Sst basin mode on the Asian summer monsoon. *Geophys. Res. Lett.*, **34**, L02708, <https://doi.org/10.1029/2006GL028571>.
- Ye, D. Z., and Y. X. Gao, 1979: *The meteorology (Tibet) Plateau*. Science Press, 278 pp. (in Chinese)
- Yeh, T.-C., S. W. Lo, and P. C. Chu, 1957: The wind structure and heat balance in the lower troposphere over Tibetan Plateau and its surrounding. *Acta Meteorologica Sinica*, **28**, 108–121, <https://doi.org/10.11676/qxxb1957.010>. (in Chinese with English abstract)
- Yu, J. H., Y. M. Liu, T. T. Ma, and G. X. Wu, 2019: Impact of surface potential vorticity density forcing over the Tibetan Plateau on the South China extreme precipitation in January 2008. Part II: Numerical simulation. *Journal of Meteorological Research*, **33**, 416–432, <https://doi.org/10.1007/s13351-019-8606-z>.
- Zhang, G. S., J. Y. Mao, G. X. Wu, and Y. M. Liu, 2021: Impact of potential vorticity anomalies around the Eastern Tibetan Plateau on Quasi-Biweekly oscillations of summer rainfall within and South of the Yangtze Basin in 2016. *Climate Dyn.*, **56**, 813–835, <https://doi.org/10.1007/s00382-020-05505-x>.
- Zhao, L. and Y. H. Ding, 2009: Potential vorticity analysis of cold air activities during the East Asian summer monsoon. *Chinese Journal of Atmospheric Sciences*, **33**, 359–374, <https://doi.org/10.3878/j.issn.1006-9895.2009.02.14>. (in Chinese with English abstract)
- Zhao, P., and L. X. Chen, 2001: Climatic features of atmospheric heat source/sink over the Qinghai-Xizang Plateau in 35 years and its relation to rainfall in China. *Science in China Series D: Earth Sciences*, **44**, 858–864, <https://doi.org/10.1007/BF02907098>.
- Zhou, X. Y., F. Liu, B. Wang, B. Q. Xiang, C. Xing, and H. Wang, 2019: Different responses of East Asian summer rainfall to El Niño decays. *Climate Dyn.*, **53**, 1497–1515, <https://doi.org/10.1007/s00382-019-04684-6>.
- Zuo, Z. Y., R. H. Zhang, and P. Zhao, 2011: The relation of vegetation over the Tibetan Plateau to rainfall in China during the boreal summer. *Climate Dyn.*, **36**, 1207–1219, <https://doi.org/10.1007/s00382-010-0863-6>.